ACS OMEGA

Article

Cite This: ACS Omega 2018, 3, 5593−5604

Novel Conducting and Biodegradable Copolymers with Noncytotoxic Properties toward Embryonic Stem Cells

Aruã C. da Silva,[†] Ana Teresa S. Semeano,[‡] André H. B. Dourado,[†] Henning Ulrich,[‡] and Susana I. Cordoba de Torresi*[,†]

[†]Department of Fundamental Chemistry, Institute of Chemistry, University of São Paulo, Av. Prof. Lineu Prestes, 748, 05508-000 São Paulo, São Paulo, Brazil

[‡]Department of Biochemistry, Institute of Chemistry, University of São Paulo, 05508-000 São Paulo, Brazil

Supporting Information

ABSTRACT: Electroactive biomaterials that are easily processed as scaffolds with good biocompatibility for tissue regeneration are difficult to design. Herein, the synthesis and characterization of a variety of novel electroactive, biodegradable biomaterials based on poly(3,4-ethylenedioxythiphene) copolymerized with poly(D,L lactic acid) (PEDOT-*co*-PDLLA) are presented. These copolymers were obtained using (2,3-dihydrothieno[3,4-*b*][1,4]dioxin-2-yl)methanol (EDOT-OH) as an initiator in a lactide ring-opening polymerization reaction, resulting in EDOT−PDLLA macromonomer. Conducting PEDOT-*co*-PDLLA copolymers (in three different proportions) were achieved by chemical copolymerization with 3,4-ethylenedioxythiophene (EDOT) monomers and persulfate oxidant. The PEDOT-*co*-PDLLA copolymers were structurally characterized by ^{1}H NMR and Fourier transform infrared spectroscopy. Cyclic voltammetry confirmed the electroactive character of the materials, and conductivity measurements were performed via electrochemical impedance spectroscopy. In vitro biodegradability was evaluated using *proteinase K* over 35 days, showing 29−46% (w/w) biodegradation. Noncytotoxicity was assessed by adhesion, migration, and proliferation assays using embryonic stem cells (E14.tg2a); excellent neuronal differentiation was observed. These novel electroactive and biodegradable PEDOT-*co*-PDLLA copolymers present surface chemistry and charge density properties that make them potentially useful as scaffold materials in different fields of applications, especially for neuronal tissue engineering.

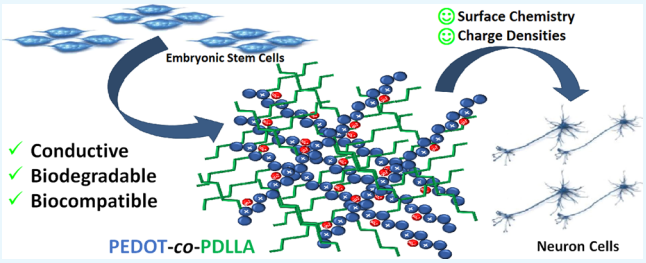

INTRODUCTION

Biomaterials play a pivotal role in the field of tissue engineering[1] and have been used to induce and accelerate various phenomena, such as tissue regeneration in wound healing;[2] rapid repair of articular cartilage with very little capacity for spontaneous healing;[3] and regeneration of damaged tissues using highly porous scaffold biomaterials[4] in bones,[5,6] the cardiovascular system,[7,8] muscles,[9,10] blood vessels,[11,12] and the neuronal system.[13−15]

Stem cells are unspecialized cells with the capacity for self-renewal and pluripotency.[16] Stem cells maintain these characteristics when grown in the presence of leukemia inhibitor factor (LIF).[17] The derivation of embryonic stem cells (ESCs) from the inner cell mass of blastocyst stage embryos was first reported in 1981.[18] ESC culture in the absence of LIF leads to the spontaneous formation of suspended cell aggregates, called embryoid bodies (EBs).[19] Once adhered, the migration of cells at the periphery of EBs is stimulated. ESCs can differentiate into the cell types of all three germ layers and give rise to any mature cell of the adult organism, making them an unlimited supply for basic research and a promising therapeutic tool for regenerative medicine.[20,21] Functional differentiated cells can potentially repair or replace tissue damaged by diseases or injuries,[22] such as diabetes, heart attack,[23] Parkinson's disease, and spinal cord injury.[24] However, protocols that allow for the better control of ESC differentiation into specific neuronal lines still require optimization. Microenvironmental mechanical properties detected by cells in contact with substrates have the ability to influence cell adhesion, migration, proliferation, and differentiation.[25,26] In recent years, there has been an increasing interest in developing materials that function as support matrices for guiding more effective cellular differentiation. These biocompatible polymeric substrates also facilitate cell transplantation because cooperation between cells is preserved, which is essential to their communication and survival.[27]

Biodegradable biomaterials are solid polymeric materials and devices that provide temporary sustentation during tissue healing procedures and enhance self-repair from injury.[28,29] Biodegradable biomaterials should not provoke sustained inflammatory or toxic responses upon implantation in the body and should have an acceptable shelf life. Their

Received: March 18, 2018
Accepted: May 8, 2018
Published: May 24, 2018

DOI: 10.1021/acsomega.8b00510
ACS Omega 2018, 3, 5593−5604

Scheme 1. (A) Synthesis of Electroactive Macromonomer EDOT−PDLLA, (B) Synthesis of Conducting and Biodegradable Copolymer PEDOT-*co*-PDLLA, and (C) Structural Representation of Copolymer with Charge on Conducting Backbone of PEDOT and Branched PDLLA Chains

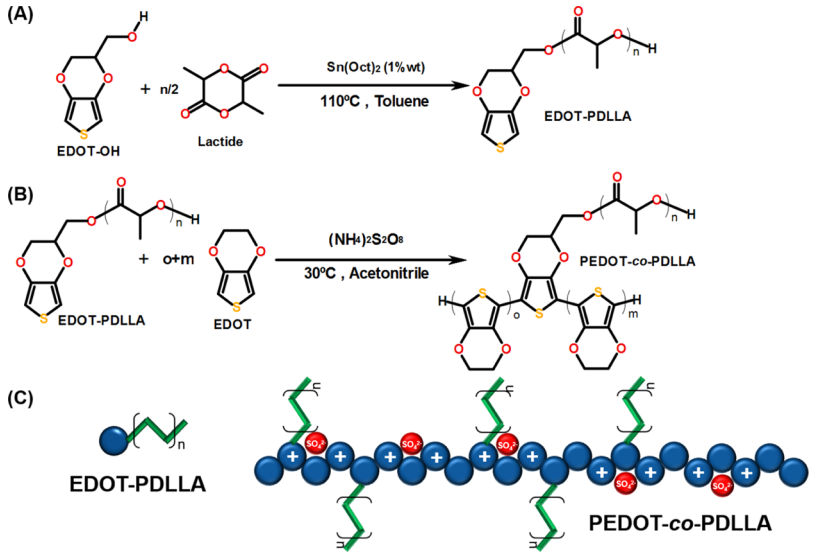

biodegradation time should match the healing or regeneration process, and furthermore, biodegradation products should be nontoxic and be metabolized and cleared from the body. Finally, biodegradable materials should have acceptable mechanical properties for the desired application.[30] In this context, biodegradable polymers based on polyesters appear to be promising candidates because of their good biocompatibility. Among these polyesters, polyglycolide,[31,32] polylactides [poly(L lactic acid) (PLLA), poly(D-lactic acid) (PDLA) or poly(D,L lactic acid) (PDLLA)],[33−35] and polycaprolactones[13,36] have been the most studied. The difference in biodegradability between PDLLA and PLLA lies in the fact that PLLA presents higher crystalline structures, which lead to lower biodegradation rates. Variations in the size and thickness of PDLLA can affect the hydrolysis rate.[37−39] Biodegradation rates can also be controlled by adjusting the molecular weight of PLA[40] or by changing the feed mole ratio of the biodegradable polymer in a copolymer composition.[41]

Electroactive biomaterials are a new generation of "smart" biomaterials based on conducting polymers (CPs).[42] Poor molecular interaction with cells is the main challenge to face for the use of CPs as biomaterials,[43] even though their biocompatibility can be highly improved by doping with specific anions[44,45] but, despite this, electroactive polymers still present low or no biodegradability.[46]

Schmidt and co-workers[47] proposed a novel biodegradable and electrical CP for biomedical applications based on a triblock polymer comprising three electroactive monomer units (polypyrrole−thiophene−polypyrrole) linked with degradable ester linkages to an aliphatic linker (4 carbons). Jing and co-workers[48] proposed a biomaterial based on a conducting and biodegradable copolymer, consisting of an aniline pentamer (AP) with a PLA triblock, called PLA-*b*-AP-*b*-PLA. Because of Jing's approach for conducting and biodegradable copolymer biomedical application, a large number of modified copolymers have been developed, such as an electroactive star-shaped memory polymer,[49] and others mainly based on aniline oligomers,[41,50] and blends with PDLLA,[51] among others.[52−56] However, polyaniline (PANI)-based polymers still show cytotoxicity because of their conductive emeraldine forms being stable only at pH levels lower than 4, thereby limiting their use in biomedical applications.[48,57,58] In this sense, other CPs, such as those based on poly(3,4-ethylenedioxythiphene) (PEDOT), arise as an alternative for biomedical applications because they are electroactive in the whole pH range.

Concerning about the role of PEDOT among the different kinds of CPs, it has emerged as the champion material in the organic bioelectronics field, both in the biosensing domain and also for integration with living cells (both in vitro and in vivo). Also, it can be synthesized in many versatile ways, such as chemical oxidative polymerization, vapor phase polymerization, or direct electrochemical polymerization, mainly as thin film to be incorporated in a wide spectrum of devices.[59]

Recently, some works presenting different strategies to achieve PEDOT derivatives such as a (bio)functional dioxythiophene monomer[60−62] have been published. Mawad and co-workers showed a functionalized PEDOT synthesized from a modified EDOT-COOH which is possible to link with hydrophilic polymers similar to PEG to obtain PEDOT hydrogels.[63] Other interesting approach was used by Zhu and co-workers which used EDOT-OH to synthesize functionalized PEDOT copolymers, formed by EDOT-PC (functionalized with phosphorylcholine) and EDOT-MI (with maleimide), with surface chemistry mimicking cell membrane with resistance to nonspecific enzyme/cell binding and recognizing target cells specifically.[64]

The challenges for developing biomaterials for active scaffolds by electrical stimulation include (1) the difficulty of working with CPs which can only be obtained over electrodes by electrochemical synthesis; (2) to achieve surface chemistry which enables surface charge keeping biocompatibility for living cells culture; and (3) poor compatibility between conducting and biodegradable polymers. Here, we report the synthesis of a novel electroactive, biodegradable, and noncytotoxic copolymer (PEDOT-*co*-PDLLA) which joins the properties of both homopolymers in a single biomaterial. This is the first report of an electroactive biodegradable biomaterial based on PEDOT,

DOI: 10.1021/acsomega.8b00510
ACS Omega 2018, 3, 5593−5604

offering the possibility of tuning conductivity and biodegradability by changing the composition.

RESULTS AND DISCUSSION

Synthesis of Conducting and Biodegradable Copolymer of PEDOT-*co*-PDLLA. The synthesis of PEDOT-*co*-PDLLA is shown in Scheme 1. The first step was the synthesis of a novel electroactive macromonomer, EDOT−PDLLA, using EDOT-OH as the initiator, and polymerizing PDLLA through a lactide ring-opening reaction catalyzed by $Sn(oct)_2$. This macromolecule corresponded to the biodegradable moiety of the copolymer. The second step was the formation of PEDOT-*co*-PDLLA at three different molar ratios, that is, 1:05, 1:25, and 1:50 PEDOT:PDLLA.

To follow the proportion of PEDOT:PDLLA in this synthesis, ^{1}H nuclear magnetic resonance (NMR) analyses were performed for all prepared copolymers (see Figure S1, Supporting Information). In the EDOT−PDLLA spectrum, at 5.25 and 1.50 ppm, the corresponding multiplet signals of CH and CH_3 of the PDLLA structure are shown. Additionally, the singlet at 6.36 ppm and a group of multiplets at 3.95−4.45 ppm are likely related to EDOT bonded to PDLLA chains. By analyzing the relative intensity of the signals, the EDOT signals are much lower than the PDLLA signals because of the higher amount of lactic acid units in the polymer compared with EDOT. A signal at 2.4 ppm was also observed in the other spectra and corresponded to the residual solvent. Regarding the PEDOT-*co*-PDLLA spectra, a singlet observed at 4.20 ppm corresponding to the CH of EDOT monomers in the PEDOT chain confirms the formation of the copolymer. By integrating the singlet at 4.20 ppm which corresponds to 2 CH present in every EDOT unit and comparing with the multiplet centered at 5.25 ppm (corresponding to CH from PDLLA), it was possible to obtain the actual molar ratio of 1:20, 1:40, and 1:80, respectively. Even though, for the whole manuscript, the feed synthesis proportion will be maintained for indicating the different copolymers.

The infrared spectra of EDOT−PDLLA and PEDOT-*co*-PDLLA at three proportions are presented (Figure S1, Supporting Information). It is possible to see that the EDOT−PDLLA spectrum presents two bands at 765 and 872 cm^{-1}, which are diminished in the polymerized structures. For a better comprehension, DFT/PBE-D3/def2-TZV was used, and the theoretical spectrum obtained presented two bands with low intensity at 765.88 and 872 cm^{-1}. These vibration groups are represented in Figure 1. Moreover, Figure S2 (Supporting Information) presents vibrations in 2998−2850 and at 1756 cm^{-1} for all spectra, corresponding to CH and CH_3 stretching and C═O, respectively, confirming the higher amounts of PDLLA in the structures.[65−67]

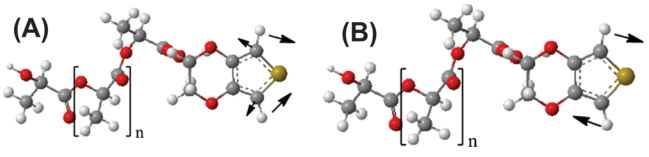

Figure 1. DFT/PBE-D3/def2-TZV optimized structures of EDOT−PDLLA macromonomers. Arrows indicate the most important contributing vibrations in the calculated band at (A) 766.88 and (B) 872 cm^{-1}.

Figure 1 shows two different vibrations that explain the results at the highlighted bands, in the macromonomer spectrum (see Figure S2, Supporting Information). The one at the lower wavenumber corresponds with the symmetrical bending of the H atoms vicinal to the S atom in EDOT. The other band, at higher energy, corresponds with the same asymmetrical bending. Because these vibrations were not present in the other molecules, this showed that these are the bonding sites to other monomers during the polymerization.

Other bands in the spectra must also be analyzed, that is, at 1090, 1130, 1190, 1450, 1640, and 1750 cm^{-1}, especially in the spectrum corresponding to the 1:25 proportion, where all of the bands are enlarged and a shoulder at 1640 cm^{-1} is clearly observed. All of these vibrations are related to the PDLLA backbone and can be assigned to ρCH_2 mode (1090 cm^{-1}), νC−C (EDOT−PDLLA) (1130 cm^{-1}), τCH_2 (1190 cm^{-1}), and δCH_2 (1450 cm^{-1}); related to the C atom in PDLLA backbone vicinal to the PEDOT one. The band at 1640 cm^{-1} is related to the νC═O mode of the segments located far away from the conductive backbone, whereas the band at 1750 cm^{-1} can be assigned to the carbonyl group of the ester segment close to the PEDOT backbone. In the spectrum of the macromonomer EDOT−PDLLA, these bands are all sharp indicating that these vibrations do not present high degree of freedom, an indication of a more rigid structure. As already mentioned, in the spectrum corresponding to the copolymers, the bands are broad and enlarged, a consequence of higher degree of interactions of the biodegradable backbones, leading to a conformation that induces the conductive backbone to be more twisted.

Electrochemical Behavior. Cyclic voltammetry was used to investigate the electrochemical behavior of the three PEDOT-*co*-PDLLA copolymers with different proportions. Figure 2 shows the *j*/*E* potentiodynamic profiles of the

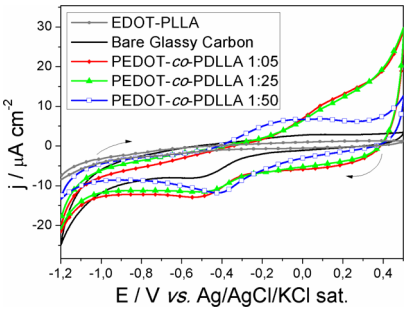

Figure 2. *j*/*E* potentiodynamic profiles of bare glassy carbon (black), EDOT−PDLLA (gray), and conducting biodegradable copolymer films of PEDOT-*co*-PDLLA 1:05 (red), 1:25 (green), and 1:50 (blue) in phosphate buffer electrolytic solution. ν = 0.01 V s^{-1}.

different films deposited onto glassy carbon electrodes. The electrochemical response of a film of the macromonomer is also presented for comparison.

Figure 2 shows the fifth voltammetric cycle of each copolymer films after stabilization in phosphoric buffer solution compared with bare vitreous carbon electrode and with a spin-coated macromonomer (EDOT−PDLLA) film. The full data with all cycles for each copolymer are shown in the Supporting Information (Figure S3). By comparing the *j*/*E* profile of the bare glassy carbon electrode with that of the macromonomer film (EDOT−PDLLA), the current generated with the macromonomer was found to be lower than that on the bare

DOI: 10.1021/acsomega.8b00510
ACS Omega 2018, 3, 5593−5604

electrode, confirming the macromonomer's insulating character. All PEDOT-*co*-PDLLA films in the three different proportions showed typical cyclic voltammograms as those observed for PEDOT, with oxidation peaks starting at −100 mV for the 1:50 copolymer and at 125 mV for the 1:25 and 1:05 copolymers and the corresponding reduction ones. The peaks appear very broad and not well-defined, but it is clear that the current is higher by increasing the EDOT/EDOT−PDLLA ratio in the copolymer formation.

Table 1 shows the conductivity values obtained by ac impedance measurements for different PEDOT-*co*-PDLLA

Table 1. Conductivity of Biodegradable and Conducting Copolymers[a]

copolymers	conductivity (S cm^{-1}) before doping	conductivity (S cm^{-1}) after doping	references
PEDOT-*co*-PDLLA 1:50		4.19×10^{-8}	present work
PEDOT-*co*-PDLLA 1:25		2.07×10^{-5}	
PEDOT-*co*-PDLLA 1:05		5.35×10^{-5}	
PUUH	0.42×10^{-8}	0.28×10^{-6}	40
PUUM	0.51×10^{-8}	0.77×10^{-6}	
PUUL	0.55×10^{-8}	1.48×10^{-6}	
PAP2		5×10^{-6}	48
EM PLAAP		1×10^{-5} to 10^{-6}	68
PEA-*g*-TA#1		7.11×10^{-7}	41
PEA-*g*-TA#2		8.01×10^{-6}	
PEA-*g*-TA#3		2.45×10^{-6}	
polypyrrole (Ppy)		1×10^{2} to 7.5×10^{3}	42
PANI		30−200	
polythiophene (PT)		$10-10^{3}$	
PEDOT:PSS		1−450	69

[a]PUUL, PUUM, and PUUH: polyurethane−urea copolymerized with an aniline trimer, doped with camphorsulfonic acid (CSA); L, M, and H related to PU molecular weight. PAP2 and EM PLAAP are both PANI pentamers doped with CSA. PEA-*g*-TA#*n*: poly(ester amide) and tetraaniline grafted poly(ester amide) copolymers. PEDOT-HA/PLLA: poly (3,4-ethylenedioxythiophene) doped with hyaluronic acid/poly (L-lactic acid) composite.

proportions compared with other conducting and biodegradable copolymers based on aniline trimers and pentamers.[40−42,48,68] The lowest PEDOT content (1:50) had conductivity comparable with undoped aniline trimers. The intermediate PEDOT content (1:25) had a slightly higher conductivity than aniline trimers doped with CSA. The highest PEDOT content (1:05) had the highest conductivity among all conducting and biodegradable copolymers, with a value 2.5 times higher than that of the 1:25 PEDOT-*co*-PDLLA. These results correlated with the voltammograms obtained from PEDOT-*co*-PDLLA films in phosphate-buffered saline (PBS) buffer. In contrast to aniline-based copolymers, which are only highly conductive at pH lower than 2 (the main problem to be solved for their application in cell interfaces), PEDOT was stable at physiological pH values of 7.4.[48,58,68] See the Supporting Information (Figure S3).

The PEDOT-*co*-PDLLA copolymers showed conductivity ranging from 4×10^{-8} to 5×10^{-5} S cm^{-1}, as shown in the Supporting Information (Figure S4) and following conductivity equation (eq 1), comparable with other biomaterials.[40−42,48,68] These conductivity values could indicate that EDOT−PDLLA macromonomers enabled the formation of copolymers with degrees of conjugation higher than aniline trimers/pentamers. On the other hand, the loss of conjugation of the conducting backbone because of steric effects related to the twisting of the PEDOT moieties functionalized with long pending PDLLA chains cannot be ignored and will lead to very low conductivities. Table 1 shows that by doubling PEDOT proportion from 1:50 to 1:25, conductivity of PEDOT-*co*-PDLLA increases 10^3 times. When PEDOT changes from 1:25 to 1:05, around the same proportion than before, conductivity increases just 2.5 times. Different effects must affect the bulk conductivity such as the increase in the degree of oligomerization together with a very twisted conducting backbone. It is already known for PANI that oligomers with 20 units already show conductivities similar to the polymeric chains[70] and the same conclusion was reached for PEDOT studies.[71] Therefore, in the present case, the slight increase in conductivity (2.5 times) for 1:25 to 1:05 must be related to a more important effect of the twisting of the chain. Even with an expected higher degree of oligomerization, a very coiled conformation would avoid conjugation as already known for PANI and polypyrrole.[70,72−74]

However, these macromonomers did not necessarily form extremely long chains as PEDOT itself. There are some experimental evidences that the formed structures were PEDOT oligomers with chain lengths that allow sufficient conjugation to achieve conductivity but were far from pure doped PEDOT chains. It must be remembered that during the oxidative synthesis in acetonitrile, only the soluble part is used. As pure PEDOT is not soluble in organic solvents, all solid precipitate is discarded. Some attempts were made to electropolymerize the macromonomer[74] but even that a rise in current is observed corresponding to the oxidation of EDOT−PLLA, no film is formed onto the electrode because of the formation of soluble oligomers. In other words, this strategy to produce a new electroactive and biodegradable biomaterial is very versatile and suggests that a branched copolymer with conducting moieties was obtained, as illustrated in Scheme 1.

Biodegradability Tests. The biodegradation behaviors of the three PEDOT-*co*-PDLLA polymers with different proportions were studied in vitro by using *proteinase K*, a high activity enzyme responsible for the biodegradation of polyesters.[75−77] Scheme 2 shows the chemical reactions for PEDOT-*co*-PDLLA copolymers and images of the PEDOT-*co*-PDLLA films before and after 35 days of biodegradation.

The biodegradation profiles of PEDOT-*co*-PDLLA films of different proportions are shown in Figure 3, from which it can be inferred that the lower the PDLLA content (higher PEDOT

Scheme 2. (A) Biodegradation Reaction and (B) Physical Aspects of PEDOT-*co*-PDLLA Films before and after 35 Days of Biodegradation Assay

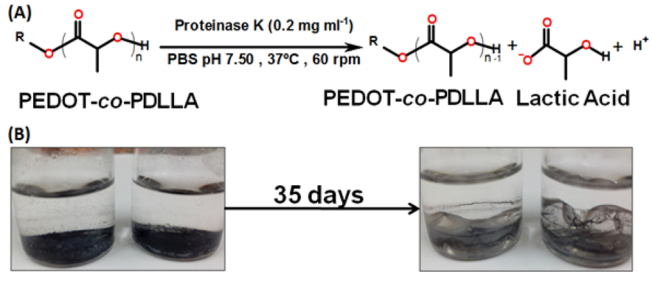

DOI: 10.1021/acsomega.8b00510
ACS Omega 2018, 3, 5593−5604

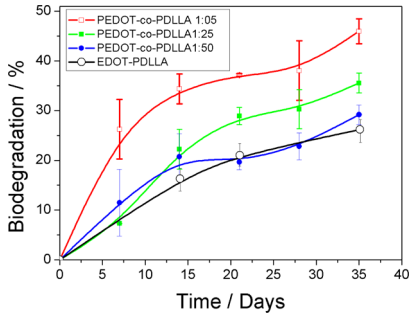

Figure 3. Biodegradation profiles of EDOT−PDLLA (black) PEDOT-*co*-PDLLA 1:05 (red), 1:25 (green), and 1:50 (blue) at 37 °C and 60 rpm.

content) is, the faster the biodegradation. The biodegradation of the macromonomer EDOT−PDLLA in the same conditions and in the same period of time is also presented.

The 1:05 copolymer (higher content of PEDOT) biodegrades much more rapidly than the others, whereas 1:25 and 1:50 do not present significant difference from macromonomer of EDOT−PDLLA, possibly because of the very low content of PEDOT in those copolymers. After 35 days, 1:05, 1:25, and 1:50 PEDOT-*co*-PDLLA copolymers reached 45.9 ± 4.1, 35.6 ± 2.0, and 29.2 ± 2.0% weight losses, respectively. Furthermore, its weight loss can be attributed to soluble components cleaved by the enzyme and water molecules (Scheme 2A), but the remaining copolymer films seem much more fragile when compared to the initial states (Scheme 2B). A few strategies for tuning biodegradation rates have included changing the number average molecular weight (M_n) of the biodegradable moiety.[40] The approach presented here employed a fixed molecular weight electroactive EDOT−PDLLA macromonomer and changed the molar ratio of EDOT−PDLLA to EDOT to obtain PEDOT-*co*-PDLLA copolymers with different biodegradation rates.

Compared with recently synthesized conducting and biodegradable copolymers presented in the literature (Table 2), the PEDOT-*co*-PDLLA copolymers displayed an acceptable range of time for biodegradation. Although our approach resulted in branched copolymers, their biodegradability behavior was closer to those obtained for aniline trimers and pentamers in block copolymers,[40,41,56] which biodegrade much more rapidly than PEDOT-HA/PLLA composites.[65] This provided strong evidence that the conducting moiety of PEDOT is composed of oligomers long enough to present electroactivity and conductivity but could be suitable for biomedical applications. These copolymers are readily consumed by macrophages during the normal wound healing response, thereby reducing the chances for long-term adverse effects.[47,78]

Water Contact Angle of PEDOT-*co*-PDLLA Films. The wettability of the different PEDOT-*co*-PDLLA copolymers were analyzed, and the results are listed in Table 3. It can be seen that the higher PDLLA content in the copolymer is, the lower the water contact angle. A polystyrene plate dish functionalized for cell culture was used as a control and had a contact angle of 28° ± 3°. The contact angle of the macromonomer EDOT−PDLLA was also measured for comparison showing a more hydrophilic character than all of the copolymers.

Cytotoxicity. Biocompatible polymers have been used to replace parts of living systems or to provide intimate contact

Table 2. Biodegradation of Conducting and Biodegradable Copolymers and Composites[a]

biomaterials	time scale (days)	biodegradation (%)	references
PEDOT-*co*-PDLLA 1:05	0−35	46	present work
PEDOT-*co*-PDLLA 1:25		36	
PEDOT-*co*-PDLLA 1:50		29	
PUUL	0−30	100	40
PUUM		50	
PUUH		10	
PH10	0−5	100	49
PH20		80	
PH40		60	
PH10AT		40	
PEA	0−6	45	41
PEA-*g*-TA#1		40	
PEA-*g*-TA#2		35	
PEA-*g*-TA#3		25	
10% PEDOT-HA/PLLA	0−56	8	65
30% PEDOT-HA/PLLA		9	
50% PEDOT-HA/PLLA		11	

[a]PUUL, PUUM, and PUUH: polyurethane−urea copolymerized with an aniline trimer; L, M, and H related to PU molecular weight. PH10, PH20, PH40, and PH10AT: star-shaped polylactide and aniline-trimer-based materials. PEA and PEA-*g*-TA#*n*: poly(ester amide) and tetraaniline grafted poly(ester amide) copolymers. PEDOT-HA/PLLA: poly (3,4-ethylenedioxythiophene) doped with hyaluronic acid/poly (L-lactic acid) composite.

Table 3. Water Contact Angle of Three Copolymers of PEDOT-*co*-PDLLA and Control

	contact angle (deg)
control	28 ± 3
PEDOT-*co*-PDLLA 1:05	64 ± 3
PEDOT-*co*-PDLLA 1:25	58 ± 1
PEDOT-*co*-PDLLA 1:50	51 ± 3
EDOT−PDLLA	47 ± 1

with living tissues. To investigate the potential biocompatibility of the PEDOT-*co*-PDLLA copolymers with biological systems, cytotoxic assays were performed with E14.tg2a ESCs using trypan blue exclusion dye (Figure 4), as were adhesion and migration assays using neural precursor cells (NPCs) sourced from predifferentiated ESCs induced by embryoid body (EB) suspension cultures (Figure 5).

Cell viability assays showed a slight decrease in proliferation of the cells grown on PEDOT-*co*-PDLLA-based polymers within the first 24 h. However, this decrease was only significant for the PEDOT:PDLLA 1:25 composition, in which a more irregular dispersion of particles occurred, possibly because of a decreased solubility. Cell viability tended to decrease by approximately 10% when cells were cultured on the copolymers compared with controls. However, this reduction was not significant for any composition.

In the absence of LIF, ESCs formed three-dimensional aggregates called EBs, which recapitulate early mammalian embryogenesis with spontaneous cell differentiation and generation of precursor cells of the three germ layers.[19] To form EBs, undifferentiated ESCs were cultured in nonadherent Petri dishes, and neuronal differentiation was induced by retinoic acid. After this stage, EBs preferentially gave rise to

DOI: 10.1021/acsomega.8b00510
ACS Omega 2018, 3, 5593−5604

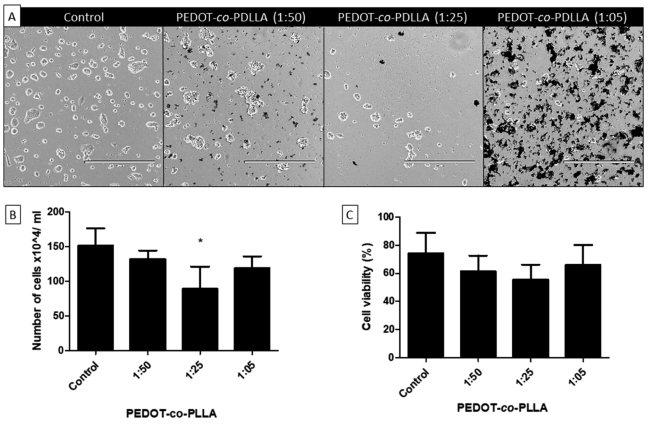

Figure 4. Proliferation and viability of ESCs on PEDOT-*co*-PDLLA CPs. Polymeric substrates with different compositions were tested against the control (traditional polystyrene plate), on which the cells were cultured for 24 h. (A) Optical microscopy images, calibration bar: 400 μm; (B) total count of cells grown on the polymer substrates; (C) percentage of viable cells shown as mean values ± SD; *P < 0.05.

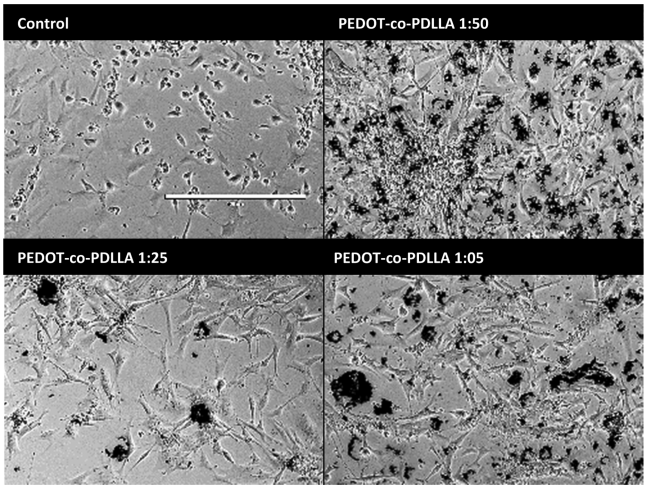

Figure 6. Phase contrast microscopy images of ESCs after 7 days of neural differentiation on PEDOT-based scaffolds. Scale bar: 400 μm.

mature neural cells as neurons and glial cells. EBs were plated on traditional plastic plates and on PEDOT-*co*-PDLLA-based polymers with PEDOT:PDLLA proportions of 1:50, 1:25, and 1:05. EBs that had adhered on the substrates were counted, and cell migration halos from the EBs were measured with ImageJ software for a minimum of 30 EBs per condition (Figure 5). Good adhesion of the EBs on the copolymers was observed; however, suitable PEDOT levels in the cell support matrix composition bring together favorable properties for adhesion of EBs, whereas higher amounts of PEDOT (i.e., composition 1:5) tended to inhibit cell adhesion and delayed cellular migration within the first 24 h. A significant decrease in the mean migration halo of adhered EBs on the PEDOT-*co*-PDLLA substrates (1:25 and 1:05) was observed compared to the controls.

The cells were induced to neuronal differentiation and assayed after 7 and 14 days. Cell morphologies after 7 days of differentiation are shown in Figure 6, and the expression patterns of neuron-specific immunomarkers are shown in Figure 7. During the differentiation progress, cells expand more on the conductive polymers than on traditional plastic, exhibiting an elongated shape with more extensive neurites.

The cells were fixed and immunostained on days 7 and 14 of the differentiation process. Immunofluorescence assays (Figures 7 and 8) showed that neuronal differentiation was enhanced by PEDOT-*co*-PDLLA coatings.

Following 7 days of induction to neural differentiation, immunostaining for βIII-tubulin, indicative of young neurons, was observed (Figure 7, first column in red). Cells cultured on conductive polymers showed higher βIII-tubulin staining and more neurite outgrowth compared to the control cell culture substrate, suggesting that the nature and surface charge density provided by the new polymeric substrates were crucial for neuronal differentiation and orientation of neuronal extensions. After 14 days of differentiation, a visible increase occurred in immunostaining for microtubule-associated protein-2 (MAP2) expression, characteristic for mature neurons (Figure 7, third column in green). This increase in MAP2 immunostaining was especially observed for the PEDOT:PDLLA 1:50 polymer, suggesting that PEDOT-*co*-PDLLA polymers promote the

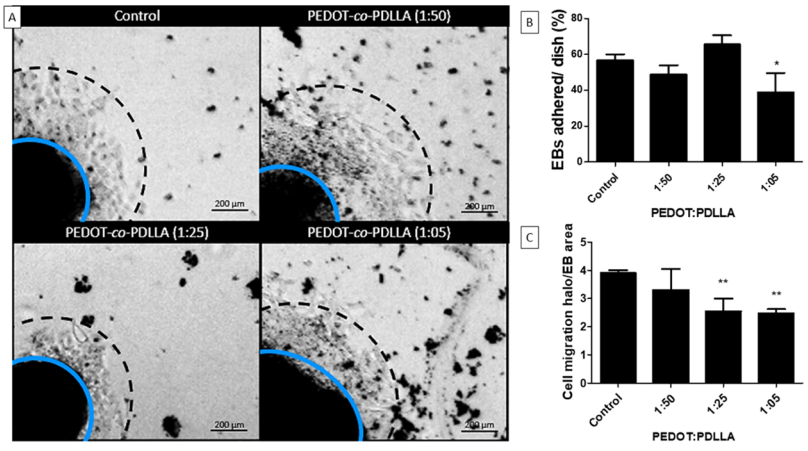

Figure 5. Adhesion and migration of NPCs from EBs on PEDOT-*co*-PDLLA CPs. Polymeric substrates for cell culture with different compositions were tested against the commercial plastic dish (control), to which the EBs adhered and the peripheral cells migrated. (A) Phase-contrast optical microscopy representative images of the EBs after 24 h of culture, with a calibration bar corresponding to 200 μm; (B) numbers of EBs adhered to the respective polymeric substrates; (C) mean ratio of the migration halo normalized by the respective area of each EB. Data are reported as mean values ± SD; *P < 0.05, **P < 0.01.

DOI: 10.1021/acsomega.8b00510
ACS Omega 2018, 3, 5593−5604

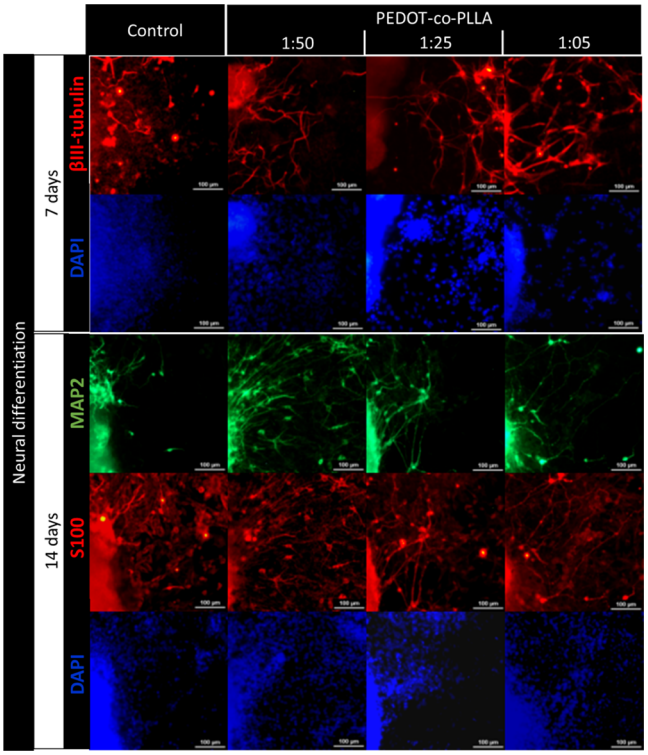

Figure 7. Characterization of E14.tg2a ESC neural differentiation on a commercial plastic plate (control) and on PEDOT:PDLLA conductive polymers at proportions of 1:50, 1:25, and 1:05. Immunostaining for young neurons with anti-βIII tubulin (red) after 7 days from the beginning of the neural differentiation process. Immunostaining for mature neurons with anti-MAP2 (green) and glial cells with anti-S100β (red) after 14 days. Cell nuclei were stained with DAPI (blue). Scale bar: 100 μm.

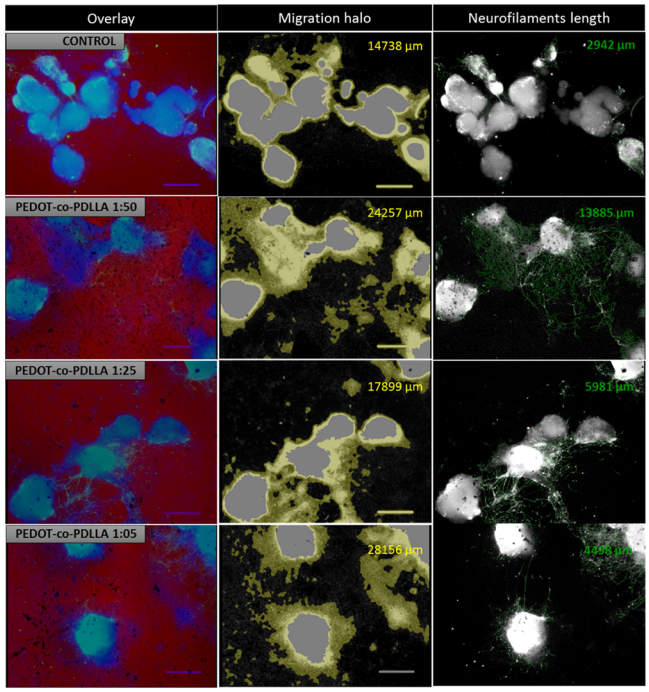

Figure 8. Quantification of neuronal-differentiated ESCs following anti-MAP-2 staining by StrataQuest analysis software (TissueGnostics). Images of phase-contrast and DAPI and Alexa488 fluorescent channels were overlaid (column 1); migration halo analysis by combining and processing images of DAPI and phase-contrast ROI (column 2); measurement of the total lengths of anti-MAP2-tagged neurites (column 3).

maturation of neurons together with neurite outgrowth, improving the complexity of the neural network. As further seen in Figure 7 in the control experiment, fewer mature neurons (MAP2-positive cells) and higher staining intensity of glial cells (anti-S100β-positive cells) were observed. This suggested that neurogenesis was favored by PEDOT-*co*-PDLLA polymer substrates.

A quantitative analysis of fluorescence images of DAPI (cell nuclei)- and MAP2-positive neural progenitor cells with Alexa 488 secondary antibody was performed using StrataQuest analysis software (TissueGnostics; Figure 8). The migration area of the cells surrounding the EBs and the total length of the neurofilaments were much larger when these agglomerated cells had adhered to the PEDOT-*co*-PDLLA matrices. The 1:50 copolymer showed the best performance in the cell culture and differentiation of neural progenitor cells, with 24 257 μm migration halos and 13 885 μm neurofilament lengths. These values represented increases of 65 and 370%, respectively, compared with controls.

DISCUSSION

Biological effects including cell adhesion, migration, and biocompatibility of a scaffold are essential for its applications in tissue engineering. Cell attachment is a crucial prerequisite for biological applications because when NPCs attached onto a scaffold under appropriate conditions, they proliferate and differentiate into different cell types.

Surface charge density promotes electrostatic interactions between the scaffold and the anchoring proteins of cells that trigger cell signaling that models cell spreading, migration, and differentiation. The orientation and adsorption rate of serum proteins in the substrate is also affected by their surface charge, interfering in the activation of integrins that feel the surrounding environment.[79]

In this context, Saltó and co-workers[80] examined whether it is possible to modulate the attachment of neural stem cells onto oxidized and reduced PEDOT/tosylate surfaces, and its results show that oxidized PEDOT increased (and reduced PEDOT decreased) the adhesion of two different types of neural stem cells. They explained that effects related to PEDOT surface in different oxidation states could dictate the orientation of proteins, hence controlling the stem cell adhesion and density. In other words, high contents of adsorbed proteins are not favorable for optimal adhesion for the two stem cell systems but rather their orientation. A dense protein layer (observed on reduced surface of PEDOT) that is tightly bound may prevent the formation of an ideal extracellular matrix onto the substrate that allows optimal interaction with cells.

Furthermore, Svennersten and co-workers[44] proposed a model to explain different effects of reduced and oxidized surfaces on cell adhesion and viability of MDCK cells on PEDOT/tosylate surface. Onto reduced surface (negative charged), fibronectin linked in an optimal structure with RGD-domains readily to bind to $\alpha_v\beta_3$ integrin, confirming that hypothesis that protein orientation plays an important role in the adhesion process. Also, they mentioned that in terms of surface chemistry, groups as $-$OH, $-$COOH, and $-NH_2$ can

DOI: 10.1021/acsomega.8b00510
ACS Omega 2018, 3, 5593−5604

bind to $\alpha_5\beta_1$ integrin, whereas $\alpha_v\beta_3$ integrin is more specific in binding to −COOH.

Because the chemical composition, stiffness, wettability, topographical, and electrical properties of the substrates can affect the biological effect of the biomaterial, it becomes difficult to identify specifically its origin;[81,82] fortunately, the comparison experiment offers some clues:

Compared with commercial polystyrene, PDLLA-based copolymers present the advantage of containing −COOH and −OH groups that improve the surface chemistry for interaction with components of the cell membrane. Besides that, during PEDOT-*co*-PDLLA synthesis, the oxidation of PEDOT with persulfate leads to positive-charged chains of PEDOT doped with SO_4^{2-} as counter-ions. Charge density increases proportionally with the PEDOT content from 1:50 to 1:05.

The nature of a charge density in CP electrodes, in analogy to that created by well-defined Helmholtz layers on metal electrodes, has to our knowledge never been described, which makes it even more complicated to understand the interface of CPs with cell culture. Because positive-charged PEDOT chains are in contact with water, proteins, and different ions in the culture media, it is possible to state that ions exchanged to counter-balance charges in PEDOT chains in a dynamic equilibrium process simultaneously with proteins adsorbing to form an adherent monolayer. This adsorption process is dominated by an entropic gain by releasing the otherwise low-entropy water that is near the interface.[83,84] Moreover, it is not well-understood if charges on the surface or electric fields generated by the motion of ions close to the interface have direct influence on cell processes such as adhesion, migration, and differentiation. However, it is well-known that cell membrane is constituted by phosphatidylserine which induced a negative charge and plays an important role in electrostatic interactions.[85] In addition, neuronal cells have negative potential in terms of balance of ions inside and outside cells,[86] and it has been widely studied in the role of electric field and stimulation on controlling ions signaling for neuronal cells.[87,88]

Undifferentiated ESCs require plasma-treated cell culture polystyrene which provides a negative charge on plastic surface encouraging cell attachment. Higher growth of ESC colonies was observed for control, followed by copolymers with the best dispersion of PEDOT, suggesting that the presence of positive charges is critical for attachment and proliferation of stem cells, in agreement with Saltó and co-workers.[80]

Surface properties as wettability and roughness play a very important role in modelling cellular adhesion. Adhesion of human fetal osteoblastic cells was enhanced on PLLA with 5 nm R_q compared to polystyrene substrates with 3.84 nm,[89] bringing evidence that the differences of nanotopography of the concerned polymers can affect these cellular processes on other cell models as neural cells.

The water contact angles of the reduced and oxidized states of PEDOT/tosylate electrode[44] are 30° ± 5° and 58° ± 6°, respectively, that are similar with contact angles of polystyrene surface (28° ± 3°) and oxidized PEDOT-*co*-PDLLA (51° to 64° dependent of PEDOT content), which suggests to be also a condition to favor the growth of neural cells on the copolymer against the control.

No obvious cytotoxicity of PEDOT-*co*-PDLLA could be observed for neural stem cells. The good performance of PEDOT-*co*-PDLLA is consistent with the previous studies of films based on both PDLLA and PEDOT which exhibited friendly interaction with neural cells. Traditional tissue cultured polystyrene plates have no charge, and data show that 7 days after retinoic acid removal and FGF and N_2 addition, the staining revealed an overall difference in βIII-tubulin positive cells which is increased when the cells are grown on PEDOT-*co*-PDLLA. Apart from excellent noncytotoxicity, it is remarkable that PEDOT-*co*-PDLLA can enhance the ESCs differentiation toward astrocytes and especially neurons. Charge and surface chemistry are key points to the improved differentiation processes.

CONCLUSIONS

The design of stimuli−response copolymers is an important developing research area of biomaterials. Such novel biomaterials should provide an optimal environment for the in vitro growth and development of cells. Herein, PEDOT-*co*-PDLLA copolymers were synthesized and presented excellent electroactivity with a wide conductivity range depending on the PEDOT content. The presence of PDLLA segments offered the copolymers biodegradability, which should be ideal for biomedical applications. In vitro cell experiments with ESCs showed that the PEDOT-*co*-PDLLA substrates were noncytotoxic and enhanced the differentiation process to neural cells. Migration halos and neurofilament lengths were increased in 65 and 370%, respectively, compared with controls, for copolymers containing 1:50 PEDOT:PDLLA; this proportion presents increased hydrophilicity and lower conductivity when compared to other copolymers with higher amount of PEDOT. As discussed, charge and surface chemistry are key points for the understanding of the mechanism of the differentiation processes. These fabricated PEDOT-*co*-PDLLA copolymers can serve as novel electroactive, biodegradable, and biocompatible materials potentially useful in different applications.

EXPERIMENTAL SECTION

Materials. (2,3-Dihydrothieno[3,4-*b*][1,4]dioxin-2-yl)-methanol (EDOT-OH) and 3,6-dimethyl-1,4-dioxane-2,5-dione (lactide) were purchased from Sigma-Aldrich. Organometallic catalyst tin(II)-2-ethylhexanoate ($Sn(oct)_2$) was obtained from Sigma-Aldrich. Toluene (99.5%), acetonitrile (99.5%), hexane (98.5%) chloroform (99.5%), and methanol (99.5%) were purchased from Synth and were distilled before use.

Chemical Synthesis of Conducting and Biodegradable Copolymers PEDOT-*co*-PDLLA. The first step of synthesis was to obtain an electroactive macromonomer of EDOT−PDLLA. 3,6-Dimethyl-1,4-dioxane-2,5-dione (2.76 g, 20 mmol), hydroxymethyl EDOT (100 mg, 0.6 mmol), and tin(II)-2-ethylhexanoate (0.016 mL, 0.05 mmol) were stirred at 110 °C with 7 mL of toluene for 24 h. The solvent was removed by distillation under reduced pressure (20 mBar, 60 °C). The obtained solid product was purified by recrystallization with a (1:4) hexane/methanol mixture, separated by decantation and vacuum dried until constant mass. The yield obtained from this procedure was 98%.

^{1}H NMR (500 MHz, $CDCl_3$-*d*): δ 1.48−1.83 (m, 3H, H^h), 3.80−3.90 (m, 2H, H^e), 4.07−4.13 (m, 1H, H^d), 4.21−4.28 (m, 2H, H^c), 5.00−5.30 (m, 1H, H^g), 6.35 (s, 2H, H^a) ppm.

^{13}C NMR (500 MHz, $CDCl_3$-*d*): δ 16.7 (C^h), 66.7 (C^c), 69.0 (C^g), 69.2 (C^e), 72.5 (C^d), 116.4 (C^a), 129.0 (C^b) 169.4 (C^f) ppm.

DOI: 10.1021/acsomega.8b00510
ACS Omega 2018, 3, 5593−5604

The second step is composed of obtaining the conducting and biodegradable copolymer of PEDOT-*co*-PDLLA. For this, 2.7 g of the macromonomer of EDOT−PDLLA was dissolved in 17.5 mL of dried acetonitrile and kept under magnetic stirring at 30 °C for 2 h. Subsequently, 3,4-ethylenedioxythiphene (EDOT) (0.06 g, 0.42 mmol; 0.12 g, 0.81 mmol; and 0.60 g, 4.20 mmol) and $NH_4S_2O_8$ (0.18 g, 0.8 mmol; 0.36 g, 1.62 mmol; and 1.80 g, 8.0 mmol) were added to the reaction vessel to obtain the proportions of 1:50, 1:25, and 1:05 of PEDOT:PDLLA, respectively, and kept under magnetic stirring at 30 °C for 24 h. After the reaction medium changed to dark blue, only the soluble fraction was placed in another glass vessel and the solvent was removed by distillation under reduced pressure (20 mBar, 60 °C), and the resultant solid obtained was PEDOT-*co*-PDLLA. Scheme 1 shows the structure and a representative illustration of PEDOT-*co*-PDLLA, as analyzed by ^{1}H and ^{13}C NMR spectroscopy.

^{1}H NMR (500 MHz, $CDCl_3$-*d*): δ 1.48−1.83 (m, 3H, H^h), 3.80−3.90 (m, 2H, H^e), 4.07−4.13 (m, 1H, H^d), 4.20 (s, 2H, CH_2ofthiophenes, H^j), 4.21−4.28 (m, 2H, H^c), 5.00−5.30 (m, 1H, H^g), 6.32 (s, 2H, H^a) ppm.

^{13}C NMR (500 MHz, $CDCl_3$-*d*): δ 16.7 (C^h), 66.7 (C^c), 69.0 (C^g), 69.2 (C^e), 72.5 (C^d), 99.0 (C-thiophene, C^j), 116.4 (C^a), 129.0 (C^b) 169.4 (C^f) ppm.

Instrumentation. ^{1}H and ^{13}C spectra were recorded on a Bruker AIII 500 MHz spectrometer at 500 and 125 MHz, respectively. Chloroform-*d* ($CDCl_3$) was used as a solvent, and tetramethylsilane served as an internal standard.

Infrared spectra were obtained with a Frontier Fourier transform infrared spectrometer (PerkinElmer) with an attenuated total reflection accessory. The spectra were captured in the 4000−600 cm^{-1} range, and an average of 32 scans was taken at a resolution of 4 cm^{-1}.

Electrochemical experiments were performed using a multipotentiostat Autolab M101 (Metrohm), controlled by NOVA 1.11 software. All experiments were performed using a platinum sheet and $Ag/AgCl/Cl^-_{(sat)}$ as counter and reference electrodes, respectively.

For electrochemical experiments, EDOT−PDLLA or PEDOT-*co*-PDLLA copolymer thin films were deposited onto glassy carbon electrodes; while for cell culture experiments, indium tin oxide (ITO)-coated glasses were used as substrates. Moreover, 20 mg/mL solutions of each copolymer or macromonomer in chloroform were prepared; then, 200 μL of each solution was slowly casted on the substrate (either glassy carbon electrode or ITO) by using an Ossila spin-coater under constant 3000 rpm rotation.

The conductivity of the copolymer films was measured by placing the copolymer films between two identical gold electrodes (diameter of 1 cm) and using a multipotentiostat Autolab M101 (Metrohm). The ac impedance was measured over a 0.01 to 10^5 Hz frequency range and an amplitude of 10 mV. The conductivity was calculated using eq 1[90]

$$\sigma = \frac{l}{RA} \tag{1}$$

where σ is the conductivity in S cm^{-1}, R is the Ohmic resistance of the copolymer, l is the distance between the two electrodes, and A is the area of the electrodes.

For biodegradation tests, a traditional procedure was employed.[76,77] The PEDOT-*co*-PDLLA copolymer films were placed in a vial 2 cm in diameter. Phosphate buffer solution was prepared at pH 7.4 and 37 °C. Each vial with copolymer film was weighed, and 5 mL of PBS, 1 mg of *proteinase K*, and 0.5 mg of chloramphenicol were added. The vials were placed in a 37 °C shaker at a rotating speed of 60 rpm. The buffer and *proteinase K* solution were replaced every 24 h to maintain the activity. Copolymer films were withdrawn every 7 days and washed twice with deionized water. Films were dried in an oven at 50 °C overnight and vacuum-dried for 2 days to remove moisture. Dry specimens were weighed, and the mass loss was calculated by the following equation

$$\text{Biodegradation (\%)} = \frac{W_0 - W_t}{W_0} \tag{2}$$

Static water contact angle measurements were used to evaluate the surface hydrophilicity of the PEDOT-*co*-PDLLA copolymers at different proportions. A drop of Milli-Q water was placed onto the surface of the sample, and a picture of the water drop was taken by a PixeLINK digital camera, coupled with Nikon optics. The images were then analyzed with ImageJ software to obtain the contact angle. The average of five measurements at different positions on the film was taken to calculate the contact angle.

In Silico Structure Optimization. The macromonomer structure was optimized by DFT calculations with ORCA 3.0.3[91] using the PBE functional[92] and atomic basis set Ahlrichs-def2-TZV,[93,94] and to consider dispersion effects, Grimme's dispersion (D3) with the Becke−Johnson damping parameter[95] was used. Hereafter, this process is named DFT/PBE-D3/def2-TZV. EDOT bonded to three units of an LA chain was used as a monomer model.

Cell Culture and Differentiation. Undifferentiated E14.tg2a mouse ESCs were cultured in high glucose Dulbecco's modified Eagle's medium (DMEM), supplemented with 1% nonessential amino acids (NEAA), 15% ESCs qualified fetal bovine serum (FBS), 7 μg/mL leukemia inhibitory factor (LIF), 100 U/mL penicillin, and 0.1 mg/mL streptomycin. EBs were formed in suspension by culturing 5 × 10^6 cells in nonadherent plates in high glucose DMEM medium without LIF and with 1% NEAA and 20% FBS for 2 days, followed by 4 days of neural differentiation induction by 2 μM retinoic acid, changing the medium every 2 days. The EBs were plated on polymer scaffolds in DMEM/F12 (1:1) medium supplemented with 20 ng/mL basic fibroblast growth factor and 1% Bottenstein's N-2 formulation to induce neuronal differentiation during 14 days. Incubation was carried under 5% CO_2 and 95% humidity at 37 °C.

Cell Viability Assay. To investigate the biocompatibility of the polymeric scaffolds with different compositions, E14.tg2a cells were seeded at a density of 1 × 10^5/cm^2 onto traditional polystyrene plates or onto copolymers films with proportions of 1:50, 1:25, and 1:05 of PEDOT:PDLLA deposited on ITO glass substrates. After 24 h, ES colonies were detached using TrypLE Express and dissociated into single cells. Dead cells were stained with 0.08% trypan blue dye mixed with cell suspension (1:1). Cell viability was determined by counting stained and unstained cells with a Neubauer chamber on an inverted microscope.

Embryoid Body Attachment and Cell Migration Assay. Cell adhesion was evaluated by the number of EBs able to attach onto the polymeric substrates. After formation and neural induction, 30 EBs were plated onto traditional plastic surfaces or PEDOT-*co*-PDLLA-based scaffolds with increasing concentrations of PEDOT. Cells were incubated at

DOI: 10.1021/acsomega.8b00510
ACS Omega 2018, 3, 5593−5604

ideal conditions for 24 h. Then, the medium with unattached EBs was changed. EBs adhered onto the polymeric surfaces were counted. To measure cell migration from the EBs, images were recorded after 48 h, and migration halos were analyzed and quantified with StrataQuest software (TissueGnostics). This imaging analysis program analyzed data obtained from tissue or cell culture slides using a workflow similar to that of flow cytometry. Gating procedures were used to determine cell populations positive or negative for epitope expression of interest. DAPI fluorescence was used as a master channel for cell quantification. Images of phase-contrast and DAPI and MAP2-staining Alexa488 fluorescence channels were overlapped. Migration halo analysis was performed by combining and processing the images of DAPI and phase-contrast ROI. Total length measurements of anti-MAP2-tagged neurites were performed.

Immunofluorescence Staining Assay. Differentiated cells were fixed with 4% paraformaldehyde in PBS for 30 min at room temperature, followed by three washes with PBS. The cells were incubated with blocking solution (0.05% Triton X-100 and 4% FBS in PBS) for 1 h and subsequently incubated with primary antibody overnight at 4 °C. The next day, PBS washes were followed by incubation with secondary antibody for 2 h at room temperature in the dark. The primary antibodies used and their dilutions were β3-tubulin and MAP2 (1:200). Alexa488 anti-rabbit and anti-mouse antibodies (1:1000) were used as secondary antibodies. The coverslips were washed three times with PBS and incubated for counterstaining with 4′,6-diamidino-2-phenyllindole (DAPI). DAPI was used as the master channel to identify nuclei.

■ ASSOCIATED CONTENT

Supporting Information

The Supporting Information is available free of charge on the ACS Publications website at DOI: 10.1021/acsomega.8b00510.

^{1}H NMR spectra, infrared spectra, *j*/*E* potentiodynamic profiles with all five cycles, and Nyquist plots of impedance spectroscopy for PEDOT-*co*-PDLLA 1:05, 1:25, and 1:50, respectively (PDF)

■ AUTHOR INFORMATION

Corresponding Author

*E-mail: storresi@iq.usp.br (S.I.C.d.T.).

ORCID

Susana I. Cordoba de Torresi: 0000-0003-3290-172X

Notes

The authors declare no competing financial interest.

■ ACKNOWLEDGMENTS

We gratefully acknowledge Brazilian agencies (São Paulo Research Foundation FAPESP, Proc. 2015/26308-7, and 2012/50880-4; National Council for Scientific and Technological Development, CNPq; and Coordination of Improvement of Higher Level Personnel, CAPES) for their financial support. A.C.d.S. and A.H.B.D. thank FAPESP (Proc. 2014/09353-6 and 2013/25592-8) for scholarships. A.T.S.S. is grateful for a CAPES graduate studies fellowship.

■ REFERENCES

(1) Hubbell, J. A. Biomaterials in Tissue Engineering. *Nat. Biotechnol.* **1995**, *13*, 565−576.

(2) Metcalfe, A. D.; Ferguson, M. W. J. Tissue Engineering of Replacement Skin: The Crossroads of Biomaterials, Wound Healing, Embryonic Development, Stem Cells and Regeneration. *J. R. Soc., Interface* **2007**, *4*, 413−437.

(3) Suh, J.-K. F.; Matthew, H. W. T. Application of Chitosan-Based Polysaccharide Biomaterials in Cartilage Tissue Engineering: A Review. *Biomaterials* **2000**, *21*, 2589−2598.

(4) O'Brien, F. J. Biomaterials & scaffolds for tissue engineering. *Mater. Today* **2011**, *14*, 88−95.

(5) Rezwan, K.; Chen, Q. Z.; Blaker, J. J.; Boccaccini, A. R. Biodegradable and Bioactive Porous Polymer/inorganic Composite Scaffolds for Bone Tissue Engineering. *Biomaterials* **2006**, *27*, 3413−3431.

(6) Hutmacher, D. W.; Schantz, J. T.; Lam, C. X. F.; Tan, K. C.; Lim, T. C. State of the Art and Future Directions of Scaffold-Based Bone Engineering from a Biomaterials Perspective. *J. Tissue Eng. Regener. Med.* **2007**, *1*, 245−260.

(7) Heydarkhan-Hagvall, S.; Schenke-Layland, K.; Dhanasopon, A. P.; Rofail, F.; Smith, H.; Wu, B. M.; Shemin, R.; Beygui, R. E.; MacLellan, W. R. Three-Dimensional Electrospun ECM-Based Hybrid Scaffolds for Cardiovascular Tissue Engineering. *Biomaterials* **2008**, *29*, 2907−2914.

(8) Balguid, A.; Mol, A.; van Marion, M. H.; Bank, R. A.; Bouten, C. V. C.; Baaijens, F. P. T. Tailoring Fiber Diameter in Electrospun Poly(ε-Caprolactone) Scaffolds for Optimal Cellular Infiltration in Cardiovascular Tissue Engineering. *Tissue Eng., Part A* **2009**, *15*, 437−444.

(9) Riboldi, S. A.; Sampaolesi, M.; Neuenschwander, P.; Cossu, G.; Mantero, S. Electrospun Degradable Polyesterurethane Membranes: Potential Scaffolds for Skeletal Muscle Tissue Engineering. *Biomaterials* **2005**, *26*, 4606−4615.

(10) Kim, B.-S.; Nikolovski, J.; Bonadio, J.; Smiley, E.; Mooney, D. J. Engineered Smooth Muscle Tissues: Regulating Cell Phenotype with the Scaffold. *Exp. Cell Res.* **1999**, *251*, 318−328.

(11) Xu, C. Aligned Biodegradable Nanofibrous Structure: A Potential Scaffold for Blood Vessel Engineering. *Biomaterials* **2004**, *25*, 877−886.

(12) Ju, Y. M.; Choi, J. S.; Atala, A.; Yoo, J. J.; Lee, S. J. Bilayered Scaffold for Engineering Cellularized Blood Vessels. *Biomaterials* **2010**, *31*, 4313−4321.

(13) Ghasemi-Mobarakeh, L.; Prabhakaran, M. P.; Morshed, M.; Nasr-Esfahani, M.-H.; Ramakrishna, S. Electrospun Poly(ε-Caprolactone)/gelatin Nanofibrous Scaffolds for Nerve Tissue Engineering. *Biomaterials* **2008**, *29*, 4532−4539.

(14) Yang, F.; Murugan, R.; Ramakrishna, S.; Wang, X.; Ma, Y.-X.; Wang, S. Fabrication of Nano-Structured Porous PLLA Scaffold Intended for Nerve Tissue Engineering. *Biomaterials* **2004**, *25*, 1891−1900.

(15) Zhong, Y.; Bellamkonda, R. V. Biomaterials for the Central Nervous System. *J. R. Soc., Interface* **2008**, *5*, 957−975.

(16) Oliveira, Á.; Corrêa-Velloso, J. d. C.; Glaser, T.; Ulrich, H. Stem Cells: Principles and Applications. *Working with Stem Cells*; Springer, 2016; pp 1−14.

(17) Smith, A. G.; Heath, J. K.; Donaldson, D. D.; Wong, G. G.; Moreau, J.; Stahl, M.; Rogers, D. Inhibition of Pluripotential Embryonic Stem Cell Differentiation by Purified Polypeptides. *Nature* **1988**, *336*, 688−690.

(18) Evans, M. J.; Kaufman, M. H. Establishment in Culture of Pluripotential Cells from Mouse Embryos. *Nature* **1981**, *292*, 154−156.

(19) Kurosawa, H. Methods for Inducing Embryoid Body Formation: In Vitro Differentiation System of Embryonic Stem Cells. *J. Biosci. Bioeng.* **2007**, *103*, 389−398.

(20) Tabar, V.; Studer, L. Pluripotent Stem Cells in Regenerative Medicine: Challenges and Recent Progress. *Nat. Rev. Genet.* **2014**, *15*, 82−92.

(21) Trounson, A.; Dewitt, N. D. Pluripotent Stem Cells Progressing to the Clinic. *Nat. Rev. Mol. Cell Biol.* **2016**, *17*, 194−200.

DOI: 10.1021/acsomega.8b00510
ACS Omega 2018, 3, 5593−5604

(22) Mahla, R. S. Stem Cells Applications in Regenerative Medicine and Disease Therapeutics. *Int. J. Cell Biol.* **2016**, *2016*, 6940283.
(23) Segers, V. F. M.; Lee, R. T. Stem-Cell Therapy for Cardiac Disease. *Nature* **2008**, *451*, 937−942.
(24) Lindvall, O.; Kokaia, Z. Stem Cells for the Treatment of Neurological Disorders. *Nature* **2006**, *441*, 1094.
(25) Murphy, W. L.; McDevitt, T. C.; Engler, A. J. Materials as Stem Cell Regulators. *Nat. Mater.* **2014**, *13*, 547−557.
(26) Semeano, A. T.; Glaser, T.; Ulrich, H. Scaffolds for Embryonic Stem Cell Growth and Differentiation. *Working with Stem Cells*; Springer, 2016; pp 347−365.
(27) Krishna, L.; Dhamodaran, K.; Jayadev, C.; Chatterjee, K.; Shetty, R.; Khora, S. S. Nanostructured Scaffold as a Determinant of Stem Cell Fate. *Stem Cell Res. Ther.* **2016**, *7*, 188.
(28) Vert, M.; Li, S. M.; Spenlehauer, G.; Guerin, P. Bioresorbability and Biocompatibility of Aliphatic Polyesters. *J. Mater. Sci.: Mater. Med.* **1992**, *3*, 432−446.
(29) Hutmacher, D. W. Scaffolds in Tissue Engineering Bone and Cartilage. *Biomaterials* **2000**, *21*, 2529−2543.
(30) Nair, L. S.; Laurencin, C. T. Biodegradable Polymers as Biomaterials. *Prog. Polym. Sci.* **2007**, *32*, 762−798.
(31) Mooney, D. Stabilized Polyglycolic Acid Fibre-Based Tubes for Tissue Engineering. *Biomaterials* **1996**, *17*, 115−124.
(32) Moutos, F. T.; Freed, L. E.; Guilak, F. A Biomimetic Three-Dimensional Woven Composite Scaffold for Functional Tissue Engineering of Cartilage. *Nat. Mater.* **2007**, *6*, 162−167.
(33) Verrier, S.; Blaker, J. J.; Maquet, V.; Hench, L. L.; Boccaccini, A. R. PDLLA/Bioglass Composites for Soft-Tissue and Hard-Tissue Engineering: An in Vitro Cell Biology Assessment. *Biomaterials* **2004**, *25*, 3013−3021.
(34) Yang, F.; Xu, C. Y.; Kotaki, M.; Wang, S.; Ramakrishna, S. Characterization of Neural Stem Cells on Electrospun poly(L-Lactic Acid) Nanofibrous Scaffold. *J. Biomater. Sci., Polym. Ed.* **2004**, *15*, 1483−1497.
(35) Yang, F.; Murugan, R.; Wang, S.; Ramakrishna, S. Electrospinning of Nano/micro Scale Poly(l-Lactic Acid) Aligned Fibers and Their Potential in Neural Tissue Engineering. *Biomaterials* **2005**, *26*, 2603−2610.
(36) Kweon, H. A Novel Degradable Polycaprolactone Networks for Tissue Engineering. *Biomaterials* **2003**, *24*, 801−808.
(37) Yang, S.; Leong, K.-F.; Du, Z.; Chua, C.-K. The Design of Scaffolds for Use in Tissue Engineering. Part I. Traditional Factors. *Tissue Eng.* **2001**, *7*, 679−689.
(38) Chen, C.-C.; Chueh, J.-Y.; Tseng, H.; Huang, H.-M.; Lee, S.-Y. Preparation and Characterization of Biodegradable PLA Polymeric Blends. *Biomaterials* **2003**, *24*, 1167−1173.
(39) Ulery, B. D.; Nair, L. S.; Laurencin, C. T. Biomedical Applications of Biodegradable Polymers. *J. Polym. Sci., Part B: Polym. Phys.* **2011**, *49*, 832−864.
(40) Chen, J.; Dong, R.; Ge, J.; Guo, B.; Ma, P. X. Biocompatible, Biodegradable, and Electroactive Polyurethane-Urea Elastomers with Tunable Hydrophilicity for Skeletal Muscle Tissue Engineering. *ACS Appl. Mater. Interfaces* **2015**, *7*, 28273−28285.
(41) Cui, H.; Liu, Y.; Deng, M.; Pang, X.; Zhang, P.; Wang, X.; Chen, X.; Wei, Y. Synthesis of Biodegradable and Electroactive Tetraaniline Grafted Poly(ester Amide) Copolymers for Bone Tissue Engineering. *Biomacromolecules* **2012**, *13*, 2881−2889.
(42) Balint, R.; Cassidy, N. J.; Cartmell, S. H. Conductive Polymers: Towards a Smart Biomaterial for Tissue Engineering. *Acta Biomater.* **2014**, *10*, 2341−2353.
(43) Ateh, D. D.; Navsaria, H. A.; Vadgama, P. Polypyrrole-Based Conducting Polymers and Interactions with Biological Tissues. *J. R. Soc., Interface* **2006**, *3*, 741−752.
(44) Svennersten, K.; Bolin, M. H.; Jager, E. W. H.; Berggren, M.; Richter-Dahlfors, A. Electrochemical Modulation of Epithelia Formation Using Conducting Polymers. *Biomaterials* **2009**, *30*, 6257−6264.
(45) Bolin, M. H.; Svennersten, K.; Wang, X.; Chronakis, I. S.; Richter-Dahlfors, A.; Jager, E. W. H.; Berggren, M. Nano-Fiber Scaffold Electrodes Based on PEDOT for Cell Stimulation. *Sens. Actuators, B* **2009**, *142*, 451−456.
(46) Bendrea, A.-D.; Cianga, L.; Cianga, I. Review Paper: Progress in the Field of Conducting Polymers for Tissue Engineering Applications. *J. Biomater. Appl.* **2011**, *26*, 3−84.
(47) Rivers, T. J.; Hudson, T. W.; Schmidt, C. E. Synthesis of a Novel, Biodegradable Electrically Conducting Polymer for Biomedical Applications. *Adv. Funct. Mater.* **2002**, *12*, 33.
(48) Huang, L.; Hu, J.; Lang, L.; Wang, X.; Zhang, P.; Jing, X.; Wang, X.; Chen, X.; Lelkes, P. I.; MacDiarmid, A. G. Synthesis and Characterization of Electroactive and Biodegradable ABA Block Copolymer of Polylactide and Aniline Pentamer. *Biomaterials* **2007**, *28*, 1741−1751.
(49) Xie, M.; Wang, L.; Ge, J.; Guo, B.; Ma, P. X. Strong Electroactive Biodegradable Shape Memory Polymer Networks Based on Star-Shaped Polylactide and Aniline Trimer for Bone Tissue Engineering. *ACS Appl. Mater. Interfaces* **2015**, *7*, 6772−6781.
(50) Dong, R.; Zhao, X.; Guo, B.; Ma, P. X. Self-Healing Conductive Injectable Hydrogels with Antibacterial Activity as Cell Delivery Carrier for Cardiac Cell Therapy. *ACS Appl. Mater. Interfaces* **2016**, *8*, 17138−17150.
(51) Jia, X.; Chao, D.; Berda, E. B.; Pei, S.; Liu, H.; Zheng, T.; Wang, C. Fabrication of Electrochemically Responsive Surface Relief Diffraction Gratings Based on a Multifunctional Polyamide Containing Oligoaniline and Azo Groups. *J. Mater. Chem.* **2011**, *21*, 18317.
(52) Guo, B.; Finne-Wistrand, A.; Albertsson, A.-C. Universal Two-Step Approach to Degradable and Electroactive Block Copolymers and Networks from Combined Ring-Opening Polymerization and Post-Functionalization via Oxidative Coupling Reactions. *Macromolecules* **2011**, *44*, 5227−5236.
(53) Guo, B.; Finne-Wistrand, A.; Albertsson, A.-C. Simple Route to Size-Tunable Degradable and Electroactive Nanoparticles from the Self-Assembly of Conducting Coil−Rod−Coil Triblock Copolymers. *Chem. Mater.* **2011**, *23*, 4045−4055.
(54) Lin, W.; Fu, Q.; Zhang, Y.; Huang, J. One-Pot Synthesis of ABC Type Triblock Copolymers via a Combination of "Click Chemistry" and Atom Transfer Nitroxide Radical Coupling Chemistry. *Macromolecules* **2008**, *41*, 4127−4135.
(55) Guo, B.; Finne-Wistrand, A.; Albertsson, A.-C. Degradable and Electroactive Hydrogels with Tunable Electrical Conductivity and Swelling Behavior. *Chem. Mater.* **2011**, *23*, 1254−1262.
(56) Borriello, A.; Guarino, V.; Schiavo, L.; Alvarez-Perez, M. A.; Ambrosio, L. Optimizing PANi Doped Electroactive Substrates as Patches for the Regeneration of Cardiac Muscle. *J. Mater. Sci.: Mater. Med.* **2011**, *22*, 1053−1062.
(57) Wang, H.-j.; Ji, L.-w.; Li, D.-f.; Wang, J.-Y. Characterization of Nanostructure and Cell Compatibility of Polyaniline Films with Different Dopant Acids. *J. Phys. Chem. B* **2008**, *112*, 2671−2677.
(58) Bober, P.; Humpolíček, P.; Pacherník, J.; Stejskal, J.; Lindfors, T. Conducting Polyaniline Based Cell Culture Substrate for Embryonic Stem Cells and Embryoid Bodies. *RSC Adv.* **2015**, *5*, 50328−50335.
(59) Strakosas, X.; Wei, B.; Martin, D. C.; Owens, R. M. Biofunctionalization of Polydioxythiophene Derivatives for Biomedical Applications. *J. Mater. Chem. B* **2016**, *4*, 4952−4968.
(60) Mantione, D.; del Agua, I.; Sanchez-Sanchez, A.; Mecerreyes, D. Poly(3,4-Ethylenedioxythiophene) (PEDOT) Derivatives: Innovative Conductive Polymers for Bioelectronics. *Polymers* **2017**, *9*, 354.
(61) Povlich, L. K.; Cho, J. C.; Leach, M. K.; Corey, J. M.; Kim, J.; Martin, D. C. Synthesis, Copolymerization and Peptide-Modification of Carboxylic Acid-Functionalized 3,4-Ethylenedioxythiophene (EDOTacid) for Neural Electrode Interfaces. *Biochim. Biophys. Acta, Gen. Subj.* **2013**, *1830*, 4288−4293.
(62) Wei, B.; Liu, J.; Ouyang, L.; Kuo, C.-C.; Martin, D. C. Significant Enhancement of PEDOT Thin Film Adhesion to Inorganic Solid Substrates with EDOT-Acid. *ACS Appl. Mater. Interfaces* **2015**, *7*, 15388−15394.
(63) Mawad, D.; Artzy-Schnirman, A.; Tonkin, J.; Ramos, J.; Inal, S.; Mahat, M. M.; Darwish, N.; Zwi-Dantsis, L.; Malliaras, G. G.;

DOI: 10.1021/acsomega.8b00510
ACS Omega 2018, 3, 5593−5604

Gooding, J. J.; et al. Electroconductive Hydrogel Based on Functional Poly(Ethylenedioxy Thiophene). *Chem. Mater.* **2016**, *28*, 6080−6088.
(64) Zhu, B.; Luo, S.-C.; Zhao, H.; Lin, H.-A.; Sekine, J.; Nakao, A.; Chen, C.; Yamashita, Y.; Yu, H.-h. Large Enhancement in Neurite Outgrowth on a Cell Membrane-Mimicking Conducting Polymer. *Nat. Commun.* **2014**, *5*, 4523.
(65) Wang, S.; Guan, S.; Wang, J.; Liu, H.; Liu, T.; Ma, X.; Cui, Z. Fabrication and Characterization of Conductive Poly (3,4-Ethylenedioxythiophene) Doped with Hyaluronic Acid/poly (L-Lactic Acid) Composite Film for Biomedical Application. *J. Biosci. Bioeng.* **2017**, *123*, 116−125.
(66) Xu, H.; Holzwarth, J. M.; Yan, Y.; Xu, P.; Zheng, H.; Yin, Y.; Li, S.; Ma, P. X. Conductive PPY/PDLLA Conduit for Peripheral Nerve Regeneration. *Biomaterials* **2014**, *35*, 225−235.
(67) Planellas, M.; Pérez-Madrigal, M. M.; del Valle, L. J.; Kobauri, S.; Katsarava, R.; Alemán, C.; Puiggalí, J. Microfibres of Conducting Polythiophene and Biodegradable Poly(ester Urea) for Scaffolds. *Polym. Chem.* **2015**, *6*, 925−937.
(68) Huang, L.; Zhuang, X.; Hu, J.; Lang, L.; Zhang, P.; Wang, Y.; Chen, X.; Wei, Y.; Jing, X. Synthesis of Biodegradable and Electroactive Multiblock Polylactide and Aniline Pentamer Copolymer for Tissue Engineering Applications. *Biomacromolecules* **2008**, *9*, 850−858.
(69) Zotti, G.; Zecchin, S.; Schiavon, G.; Louwet, F.; Groenendaal, L.; Crispin, X.; Osikowicz, W.; Salaneck, W.; Fahlman, M. Electrochemical and XPS Studies toward the Role of Monomeric and Polymeric Sulfonate Counterions in the Synthesis, Composition, and Properties of Poly(3,4-Ethylenedioxythiophene). *Macromolecules* **2003**, *36*, 3337−3344.
(70) MacDiarmid, A. G.; Zhou, Y.; Feng, J. Oligomers and Isomers: New Horizons in Poly-Anilines. *Synth. Met.* **1999**, *100*, 131−140.
(71) Elliott, B. J.; Ellis, W. W.; Luebben, S. D.; Sapp, S. A.; Chang, C.-H.; D'Sa, R. Electrically Conducting Materials from Branched End-Capping Intermediates. U.S. Patent 7,361,728 B1, 2004.
(72) MacDiarmid, A. G. Polyaniline and Polypyrrole: Where Are We Headed? *Synth. Met.* **1997**, *84*, 27−34.
(73) Avlyanov, J. K.; Min, Y.; MacDiarmid, A. G.; Epstein, A. J. Polyaniline: Conformational Changes Induced in Solution by Variation of Solvent and Doping Level. *Synth. Met.* **1995**, *72*, 65−71.
(74) da Silva, A. C.; Augusto, T.; Andrade, L. H.; de Torresi, S. I. C. One Pot Biocatalytic Synthesis of a Biodegradable Electroactive Macromonomer Based on 3,4-Ethylenedioxytiophene and Poly(L-Lactic Acid). *Mater. Sci. Eng., C* **2018**, *83*, 35−43.
(75) Betzel, C.; Singh, T. P.; Visanji, M.; Peters, K.; Fittkau, S.; Saenger, W.; Wilson, K. S. Structure of the Complex of Proteinase K with a Substrate Analogue Hexapeptide Inhibitor at 2.2-A Resolution. *J. Biol. Chem.* **1993**, *268*, 15854−15858.
(76) Singh, N. K.; Singh, S. K.; Dash, D.; Gonugunta, P.; Misra, M.; Maiti, P. CNT Induced β-Phase in Polylactide: Unique Crystallization, Biodegradation, and Biocompatibility. *J. Phys. Chem. C* **2013**, *117*, 10163−10174.
(77) Morihara, K.; Tsuzuki, H. Specificity of Proteinase K from Tritirachium Album Limber for Synthetic Peptides. *Agric. Biol. Chem.* **1975**, *39*, 1489−1492.
(78) Green, T. R.; Fisher, J.; Matthews, J. B.; Stone, M. H.; Ingham, E. Effect of Size and Dose on Bone Resorption Activity of Macrophages by in Vitro Clinically Relevant Ultra High Molecular Weight Polyethylene Particles. *J. Biomed. Mater. Res.* **2000**, *53*, 490−497.
(79) Hayashi, Y.; Furue, M. K.; Okamoto, T.; Ohnuma, K.; Myoishi, Y.; Fukuhara, Y.; Abe, T.; Sato, J. D.; Hata, R.-I.; Asashima, M. Integrins Regulate Mouse Embryonic Stem Cell Self-Renewal. *Stem Cells* **2007**, *25*, 3005−3015.
(80) Saltó, C.; Saindon, E.; Bolin, M.; Kanciurzewska, A.; Fahlman, M.; Jager, E. W. H.; Tengvall, P.; Arenas, E.; Berggren, M. Control of Neural Stem Cell Adhesion and Density by an Electronic Polymer Surface Switch. *Langmuir* **2008**, *24*, 14133−14138.
(81) Li, N.; Zhang, Q.; Gao, S.; Song, Q.; Huang, R.; Wang, L.; Liu, L.; Dai, J.; Tang, M.; Cheng, G. Three-Dimensional Graphene Foam as a Biocompatible and Conductive Scaffold for Neural Stem Cells. *Sci. Rep.* **2013**, *3*, 1604.
(82) Snydman, D. R.; Walker, M.; Kublin, J. G.; Zunt, J. R. Parasitic Central Nervous System Infections in Immunocompromised Hosts: Malaria, Microsporidiosis, Leishmaniasis, and African Trypanosomiasis. *Clin. Infect. Dis.* **2006**, *42*, 115−125.
(83) Sanfeld, A.; Royer, C.; Steinchen, A. Thermodynamic, Kinetic and Conformational Analysis of Proteins Diffusion−sorption on a Solid Surface. *Adv. Colloid Interface Sci.* **2015**, *222*, 639−660.
(84) Norde, W. Protein Adsorption at Solid Surfaces: A Thermodynamic Approach. *Pure Appl. Chem.* **1994**, *66*, 491.
(85) Yeung, T.; Gilbert, G. E.; Shi, J.; Silvius, J.; Kapus, A.; Grinstein, S. Membrane Phosphatidylserine Regulates Surface Charge and Protein Localization. *Science* **2008**, *319*, 210−213.
(86) White, G.; Lovinger, D. M.; Weight, F. F. Transient Low-Threshold Ca2+ Current Triggers Burst Firing through an After-depolarizing Potential in an Adult Mammalian Neuron. *Proc. Natl. Acad. Sci. U.S.A.* **1989**, *86*, 6802−6806.
(87) Monteith, G. R.; McAndrew, D.; Faddy, H. M.; Roberts-Thomson, S. J. Calcium and Cancer: Targeting Ca2+ Transport. *Nat. Rev. Cancer* **2007**, *7*, 519−530.
(88) Isaksson, J.; Kjäll, P.; Nilsson, D.; Robinson, N.; Berggren, M.; Richter-Dahlfors, A. Electronic Control of Ca2+ Signalling in Neuronal Cells Using an Organic Electronic Ion Pump. *Nat. Mater.* **2007**, *6*, 673−679.
(89) Taylor, A. C.; González, C. H.; Miller, B. S.; Edgington, R. J.; Ferretti, P.; Jackman, R. B. Surface Functionalisation of Nanodiamonds for Human Neural Stem Cell Adhesion and Proliferation. *Sci. Rep.* **2017**, *7*, 7307.
(90) Gao, M.; Wang, Y.; Yi, Q.; Su, Y.; Sun, P.; Wang, X.; Zhao, J.; Zou, G. A Novel Solid-State Electrolyte Based on a Crown Ether Lithium Salt Complex. *J. Mater. Chem. A* **2015**, *3*, 20541−20546.
(91) Neese, F. The ORCA Program System. *Wiley Interdiscip. Rev.: Comput. Mol. Sci.* **2012**, *2*, 73−78.
(92) Perdew, J. P.; Burke, K.; Ernzerhof, M. Generalized Gradient Approximation Made Simple. *Phys. Rev. Lett.* **1996**, *77*, 3865−3868.
(93) Schäfer, A.; Horn, H.; Ahlrichs, R. Fully Optimized Contracted Gaussian Basis Sets for Atoms Li to Kr. *J. Chem. Phys.* **1992**, *97*, 2571.
(94) Weigend, F.; Ahlrichs, R. Balanced Basis Sets of Split Valence, Triple Zeta Valence and Quadruple Zeta Valence Quality for H to Rn: Design and Assessment of Accuracy. *Phys. Chem. Chem. Phys.* **2005**, *7*, 3297−3305.
(95) Grimme, S.; Ehrlich, S.; Goerigk, L. Effect of the Damping Function in Dispersion Corrected Density Functional Theory. *J. Comput. Chem.* **2011**, *32*, 1456−1465.

DOI: 10.1021/acsomega.8b00510
ACS Omega 2018, 3, 5593−5604